Genetic Disruption of Myostatin Reduces the Development of Proatherogenic Dyslipidemia and Atherogenic Lesions In *Ldlr* Null Mice

Powen Tu,[1] Shalender Bhasin,[1,2] Paul W. Hruz,[3] Karen L. Herbst,[4] Lawrence W. Castellani,[5] Ning Hua,[6] James A. Hamilton,[6] and Wen Guo[2]

OBJECTIVE—Insulin-resistant states, such as obesity and type 2 diabetes, contribute substantially to accelerated atherogenesis. Null mutations of myostatin (*Mstn*) are associated with increased muscle mass and decreased fat mass. In this study, we determined whether *Mstn* disruption could prevent the development of insulin resistance, proatherogenic dyslipidemia, and atherogenesis.

RESEARCH DESIGN AND METHODS—C57BL/6 $Ldlr^{-/-}$ mice were cross-bred with C57BL/6 $Mstn^{-/-}$ mice for >10 generations to generate $Mstn^{-/-}/Ldlr^{-/-}$ double-knockout mice. The effects of high-fat/high-cholesterol diet on body composition, plasma lipids, systemic and tissue-specific insulin sensitivity, hepatic steatosis, as well as aortic atheromatous lesion were characterized in $Mstn^{-/-}/Ldlr^{-/-}$ mice in comparison with control $Mstn^{+/+}/Ldlr^{-/-}$ mice.

RESULTS—Compared with $Mstn^{+/+}/Ldlr^{-/-}$ controls, $Mstn^{-/-}/Ldlr^{-/-}$ mice were resistant to diet-induced obesity, and had greatly improved insulin sensitivity, as indicated by 42% higher glucose infusion rate and 90% greater muscle [^{3}H]-2-deoxyglucose uptake during hyperinsulinemic-euglycemic clamp. $Mstn^{-/-}/Ldlr^{-/-}$ mice were protected against diet-induced hepatic steatosis and had 56% higher rate of hepatic fatty acid β-oxidation than controls. $Mstn^{-/-}/Ldlr^{-/-}$ mice also had 36% lower VLDL secretion rate and were protected against diet-induced dyslipidemia, as indicated by 30–60% lower VLDL and LDL cholesterol, free fatty acids, and triglycerides. Magnetic resonance angiography and *en face* analyses demonstrated 41% reduction in aortic atheromatous lesions in $Ldlr^{-/-}$ mice with *Mstn* deletion.

CONCLUSIONS—Inactivation of *Mstn* protects against the development of insulin resistance, proatherogenic dyslipidemia, and aortic atherogenesis in $Ldlr^{-/-}$ mice. Myostatin may be a useful target for drug development for prevention and treatment of obesity and its associated type 2 diabetes and atherosclerosis.
***Diabetes* 58:1739–1748, 2009**

From the [1]Department of Molecular Medicine, Boston University School of Medicine, Boston, Massachusetts; the [2]Section of Endocrinology, Diabetes, & Nutrition, Department of Medicine, Boston Medical Center, Boston, Massachusetts; the [3]Department of Pediatrics, Washington University School of Medicine, St. Louis, Missouri; the [4]Division of Endocrinology & Metabolism, University of California San Diego, San Diego, California; the [5]Departments of Medicine/Cardiology, University of California Los Angeles, Los Angeles, California; and the [6]Department of Physiology and Biophysics, Boston University School of Medicine, Boston, Massachusetts.

Corresponding author: Shalender Bhasin, bhasin@bu.edu.

Received 6 March 2009 and accepted 12 May 2009.

Published ahead of print at http://diabetes.diabetesjournals.org on 9 June 2009. DOI: 10.2337/db09-0349.

Heart disease and diabetes rank among the most prevalent disorders in most Western countries, and their incidence rates within the elderly population are particularly high (1). Aging is associated with decrease in muscle mass, increase in fat mass (2), insulin resistance, and atherosclerosis progression, all conditions that predispose individuals to cardiometabolic diseases. Therefore, adiposity, sarcopenia, and heart disease are interrelated consequences of aging that contribute substantially to morbidity and mortality among older humans.

Currently, most available therapies for heart disease, such as statins, are based on lowering of plasma cholesterol. These interventions have little effect on adiposity and sarcopenia. We surmised that unlike available pharmacological therapies that are mostly targeted at cholesterol synthesis or metabolism, novel therapeutic strategies, such as myostatin inactivation, that directly target muscle and fat mass accumulation may be effective in protection against obesity and its metabolic ramifications.

Genetic disruption of myostatin, a transforming growth factor-β (TGF-β) family member that functions as an endogenous inhibitor of muscle growth (3–5), leads to increased skeletal muscle mass and decreased fat mass in humans, cattle, mice, and other species (6,7). Disruption of myostatin gene has also been shown to prevent the development of obesity (6). Inhibition of myostatin, either directly or through overexpression of myostatin propeptide, an endogenous myostatin inhibitor, has also been shown to prevent the development of obesity and insulin resistance (6).

In this study, we show that the loss of myostatin attenuates the development of atherogenic lipid profile and the progression of atheromatous lesion growth in LDL receptor–null ($Ldlr^{-/-}$) mice, a widely used experimental model of atherogenesis. When $Ldlr^{-/-}$ mice, lacking the cell-surface transmembrane receptor that recognizes apolipoprotein B100 (apoB100), are fed Western-type diet, they display hypercholesterolemia and atheromatous lesions resembling those observed in patients with familial hypercholesterolemia (8). Our data show that *Mstn* disruption in $Ldlr^{-/-}$ mice not only attenuates diet-induced fat accumulation and improves whole body insulin sensitivity, as has been reported recently (9,10), but it also prevents the hepatic hypersecretion of proatherogenic lipoprotein, protects against the development of proatherogenic dyslipidemia, and reduces atherogenesis progression.

RESEARCH DESIGN AND METHODS

C57BL/6 mice with homozygous deletion of *Ldlr* (Jackson Laboratory, Bar Harbor, ME) were cross-bred with C57BL/6 mice with homozygous deletion of *Mstn*. Their offsprings were bred >10 times to generate $Mstn^{-/-}/Ldlr^{-/-}$ double-knockout mice. All mice used in this study were males. Mice were provided food and water ad libitum and maintained on a 12-h light/dark cycle. Mice were fed normal rodent diet (TD#2018, Harland Teklad, Madison, WI) until 4 months of age, then fed with high-fat/high-cholesterol diet (HFD) (TD#94059, Harland Teklad). The HFD contained 15.8% w/w fat (primarily from cocoa butter), 1.25% w/w cholesterol, 41.2% w/w carbohydrate, and 19.7% w/w protein. Food consumption was measured using powdered HFD provided in glass jars with perforated metal tops to prevent scattering. Study protocols were approved by the Boston University's Institutional Animal Care and Use Committee.

Body composition and metabolic cage measurements. Whole body fat and muscle mass were determined by nuclear magnetic resonance (NMR; EchoMRI-100, Echo Medical System, Houston, TX). Visceral and subcutaneous fat imaging were performed using low-energy X-ray micro–computed tomography (CT) scanner (LaTheta LCT-100A, Echo Medical System). Oxygen consumption and respiratory exchange ratio rates were measured using Oxymax system (Columbus Instruments, Columbus, OH) as previously described (11).

Magnetic resonance angiography. Mice were anesthetized using 1–2% (v/v) isoflurane and 1–2 L/min oxygen flow through an anesthesia monitoring system (Smiths Medical PM, Waukesha, WI). Respiration was monitored by respiration sensor pillow (SA Instruments, Stony Brook, NY). Imaging was performed using a Bruker Avance 500 vertical bore spectrometer with 11.7 T (Bruker, Billerica, MA). Data acquisition and reconstruction were performed with the ParaVision 3.0.2. 3D magnetic resonance angiography (MRA) and were obtained using the FLASH_3D_ANGIO pulse sequence (flip angle = 20°, TE/TR = 2.18 ms/20 ms, FOV = 15 mm × 15 mm × 15 mm). Four averages were obtained in each scan.

***En face* detection of atheromatous lesions.** Preparation of aortas and quantification of atheromatous lesions were performed in animals after 12 weeks of HFD feeding, using procedures previously described (12). The heart with aorta was embedded in optimal cutting temperature (OCT) (Sakura Finetech USA, Torrance, CA), and serial 10 μm-thick cytosections of aortic root were stained with Oil Red O by the Rodent Histopathology Core at Harvard Medical School (Boston, MA).

Measurements of plasma lipids and other metabolites. Blood glucose and ketone concentrations were determined using Glucometer Elite XL (Bayer, Tarrytown, NY) and Precision Xtra (Abbott Laboratories, Bedford, MA), respectively. Plasma insulin and glucagon were measured using ultrasensitive ELISA (Alpco, Salem, NH). For lipid analyses, fasting (food removed for 12 h) and nonfasting (food removed for 3 h) blood samples were collected from the retro-orbital plexus under isoflurane anesthesia. Lipid analyses were performed using procedures previously described (13). Cholesterol and triglyceride distribution of the lipoproteins were performed by Cardiovascular Specialty Laboratories (Atlanta, GA) using fast-performance liquid chromatography (14). Fractions 2–6 contain VLDL; fractions 7–11 contain LDL; and fractions 14–17 contain HDL.

Glucose and insulin tolerance tests. For glucose tolerance tests, fasting mice were given D-glucose (1 g/kg) by intraperitoneal injection. For insulin tolerance tests, nonfasting mice were given insulin (0.75 IU/kg) (Eli Lilly, Indianapolis, IN) by intraperitoneal injection. Blood glucose was measured using Glucometer Elite XL (Bayer).

Hyperinsulinemic-euglycemic clamp studies. Hyperinsulinemic-euglycemic clamps were performed by a modification of a described procedure (15). Briefly, right jugular vein of killed mice (80–10 mg/kg ketamine-xylazine i.p.) was catheterized with heparin-coated MRE-025 tubing (Becton Dickinson, Franklin Lakes, NJ). Animals were allowed to recover for 1–2 days. Insulin (10 $mU \cdot kg^{-1} \cdot min^{-1}$) containing 0.3% BSA was infused at the rate of 1 μl/min using a syringe pump (HA11D, Harvard apparatus, Holliston, MA). At 5-min intervals, ~2 μl of tail vein blood was drawn to measure blood glucose. Dextrose (25%) was infused at a rate sufficient to maintain blood glucose of 140 mg/dl. Average glucose infusion rate (GIR) was measured over the final 30 min of the 2-h clamp. Insulin was measured in blood samples from the last three collections.

Muscle [^{3}H]-2-deoxyglucose uptake. Muscle uptake of the metabolically inert glucose analog, [^{3}H]-2-deoxyglucose (DOG), was performed in mice at 30 min before the end of 2-h hyperinsulinemic-euglycemic clamp experiments, with modification to methods described previously (15). Briefly, DOG (30 μCi) was administered intraperitoneally, and mouse hind-limb muscles were harvested, denatured, and the eluates were quantified using liquid scintillation analyzer (TriCarb 3100TR, PerkinElmer, Shelton, CT). The rate of glucose uptake was calculated by dividing the muscle DOG uptake over a 30-min interval (cpm · kg^{-1} · min^{-1}) by the mean blood glucose–specific activity (glucose cpm/mg).

Histology. Liver tissues were embedded in OCT. Serial 10 μm-thick cytosections were prepared at the Rodent Histopathology Core at Harvard Medical School (Boston, MA) and were stained with Oil Red O and hematoxylin-eosin.

Intrahepatic lipid measurements. Livers were lyophilized using Freeze Dry System (Freezone, Labconco, Fort Scott, KS) to obtain liver dry weight. Liver lipids were extracted by the Folch method (16). Liver cholesterol and triglycerides were measured using Infinity Cholesterol (Thermo Electron, Pittsburgh, PA) and T2449 Triglyceride Reagent (Sigma Aldrich, St. Louis, MO), respectively.

Mitochondrial fatty acid β-oxidation measurement. Fresh liver tissue was homogenized in 250 mmol/l sucrose, 0.1 mmol/l EDTA, 50 mmol/l KCl, and 10 mmol/l HEPES (pH 7.4) and centrifuged at 1,000 × *g* for 5 min. The supernatant was centrifuged at 10,000 × *g* for 15 min, and pellets were dissolved in 50 mmol/l KCl, 70 mmol/l sucrose, 3.6 mmol/l $MgCl_2$, 7.2 mmol/l K_2HPO_4, and 36 mmol/l Tris-HCl (pH 7.4). Protein concentrations were measured using Bradford reagent (Bio-Rad, Hercules, CA). In addition, 5 μCi/ml [^{3}H]-palmitate was incubated with 1 mg of mitochondria in preincubation buffer with 2 mmol/l KCN at room temperature for 30 min. Reaction was subsequently incubated for 60 min in 5% perchloric acid, and supernatants were counted in a liquid scintillation counter.

Hepatic VLDL (apoB100) secretion. VLDL secretion rate was measured by modification of a previously described method (17). Briefly, fasted mice were injected with Triton WR 1339 (500 mg/kg; Sigma Chemical, St. Louis, MO) via tail vein to block lipolysis. Blood samples were collected at baseline, 90 min and 180 min after injection. Plasma apoB100 was determined by Western blot analysis using anti-apoB antibody (Santa Cruz Biotechnology, Santa Cruz, CA). Hepatic VLDL secretion was calculated by the percentage increase in plasma apoB100 from baseline.

Western blot analysis. One microliter of plasma per lane was analyzed after treatment with sample buffer containing SDS and β-mercaptoethanol, followed by separation in 4–15% Tris-HCl gradient gel (Bio-Rad, Hercules, CA). Liver and muscle tissue samples were extracted and processed as previously described (12). All primary, except anti–fatty acid synthase antibodies (Cell Signaling Technology, Danvers, MA), and secondary antibodies were purchased from Santa Cruz Biotechnnology.

Real-time Q-PCR. Total RNA was extracted from frozen liver using RNeasy mini kit (Qiagen, Valencia, CA). For reverse transcription, 1 μg of the total RNA was converted to first-strand complementary DNA in 20 μl reactions using AffinityScript Q-PCR cDNA Synthesis Kit (Agilent Technologies, La Jolla, CA), which was subsequently diluted five times. For PCR sample preparation, 5 μl of cDNA was mixed in 20 μl reaction volume with 10 μmol/l primer and SYBR master enzyme mix (SABiosciences, Frederick, MD). The reaction was initiated at 94°C for 10 min, followed by 40 cycles through 94°C × 15 s and 60°C × 1 min. All reactions were performed in duplicate. All CT values were in the range of 20–30 cycles. Amplification curves were analyzed using SDS 1.9.1 software (Applied Biosystems, Foster City, CA). *Hprt1* controls provided relative gene expression levels. Refer to supplementary Table 1 (available in an online appendix at http://diabetes.diabetesjournals.org/cgi/content/full/db09-0349/DC1) for primers.

Statistical analysis. Experimental results are shown as means ± SE. The mean values from two independent groups were compared by using Student's *t* test for independent samples. Differences among multiple groups were assessed using ANOVA models. If ANOVA revealed a significant overall effect, then individual groups were compared by using Tukey's procedure. Longitudinal data from multiple groups of animals were compared by using repeated measures ANOVA, with a time-in-treatment factor and a treatment group factor. All statistical tests were one-tailed and $P < 0.05$ were considered significant.

RESULTS

***Mstn* deletion retards whole body, visceral, and subcutaneous fat accumulation.** $Ldlr^{-/-}$ mice with varying *Mstn* genotypes, wild type ($Mstn^{+/+}/Ldlr^{-/-}$), heterozygous deletion ($Mstn^{+/-}/Ldlr^{-/-}$), and homozygous deletion ($Mstn^{-/-}/Ldlr^{-/-}$), were fed HFD for 11–12 weeks. $Mstn^{+/+}/Ldlr^{-/-}$ controls demonstrated substantial gains in body weight, whole body fat mass (measured by NMR), and visceral and subcutaneous fat mass (measured by micro-CT scan). In contrast, $Mstn^{-/-}/Ldlr^{-/-}$ mice resisted weight gain and accumulation of whole body and visceral fat mass in response to HFD (Fig. 1*A* and *B*, supplementary Fig. 1*A* and *B*, available in an online

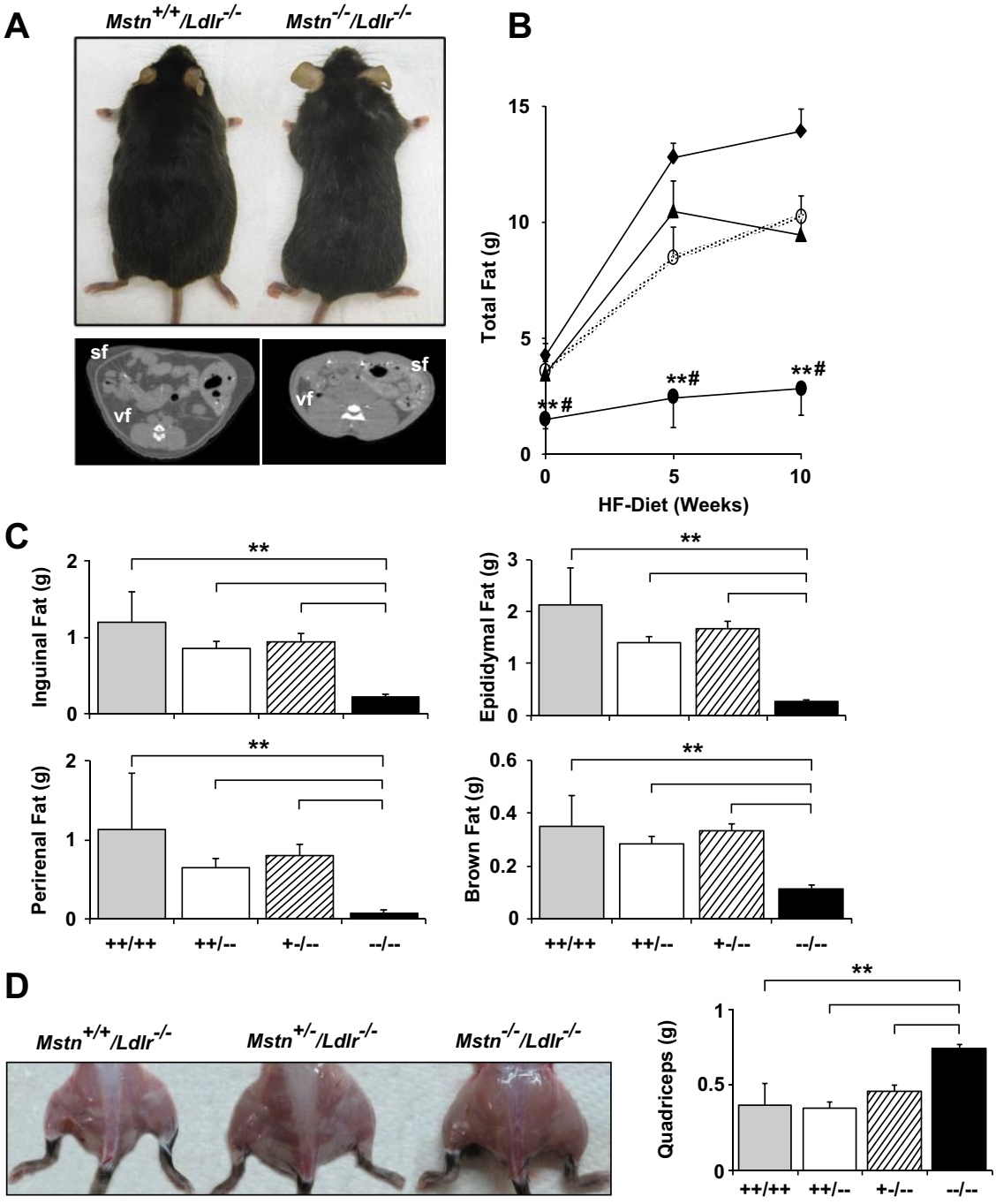

FIG. 1. Effects of *Mstn* disruption on body fat accumulation in $Ldlr^{-/-}$ mice. *A*: Representative gross appearance (*top panel*) and micro-CT image of visceral and subcutaneous fat (*bottom panel*) of mice after 12 weeks of HFD (HF-diet). c, cecum; vf, visceral fat, sf, subcutaneous fat. *B*: NMR analysis of total fat at baseline (time 0) and after 5 and 10 weeks of HFD. $Mstn^{+/+}/Ldlr^{+/+}$, ♦; $Mstn^{+/+}/Ldlr^{-/-}$, ○; $Mstn^{+-}/Ldlr^{-/-}$, ▲; $Mstn^{+-}/Ldlr^{-/-}$, ●. *C*: Inguinal, epididymal, perirenal, and intrascapular brown fat weights of mice after 12 weeks of HFD. *D*: Representative gross appearance of hind-limb muscles (*left panel*) and quadriceps muscle weights (*right panel*) of mice after 12 weeks of HFD. ++/++, $Mstn^{+/+}/Ldlr^{+/+}$. $^{++/-}$, $Mstn^{+/+}/Ldlr^{-/-}$. $^{+-/--}$, $Mstn^{+-}/Ldlr^{-/-}$. $^{--/--}$, $Mstn^{-/-}/Ldlr^{-/-}$. Data are expressed as means ± SE (n = 11–21). $^{**}P <$ 0.01 compared with all other genotypes. (A high-quality digital representation of this figure is available in the online issue.)

appendix). In agreement with the in vivo NMR data, the wet weights of the major fat depots (inguinal, epididymal, perirenal, as well as the interscapular brown fat) were significantly lower in the $Mstn^{-/-}/Ldlr^{-/-}$ mice, as compared with wild-type, $Mstn^{+/+}/Ldlr^{-/-}$, and $Mstn^{+/-}/Ldlr^{-/-}$ mice (Fig. 1*C*). Thus, $Mstn^{-/-}/Ldlr^{-/-}$ mice are resistant to fat accumulation in all fat depots including the visceral and subcutaneous fat depot.

As expected, the $Mstn^{-/-}/Ldlr^{-/-}$ mice had significantly greater skeletal muscle mass, as indicated by the twofold higher mass of the *gastrocnemius* and the *quadriceps femoris* muscle groups (Fig. 1*D*; supplementary Fig. 1*C* and *D*, available in an online appendix) than in the $Mstn^{+/+}/Ldlr^{-/-}$ controls. Throughout the course of HFD, $Mstn^{-/-}/Ldlr^{-/-}$ mice maintained significantly greater lean mass (assessed by NMR) compared with other genotype groups (Fig. 1*D*; supplementary Fig. 1*C*, available in an online appendix). The *soleus* muscle, a primarily oxidative muscle type, was not statistically significantly affected by *Mstn* disruption (supplementary Fig. 1*E*,

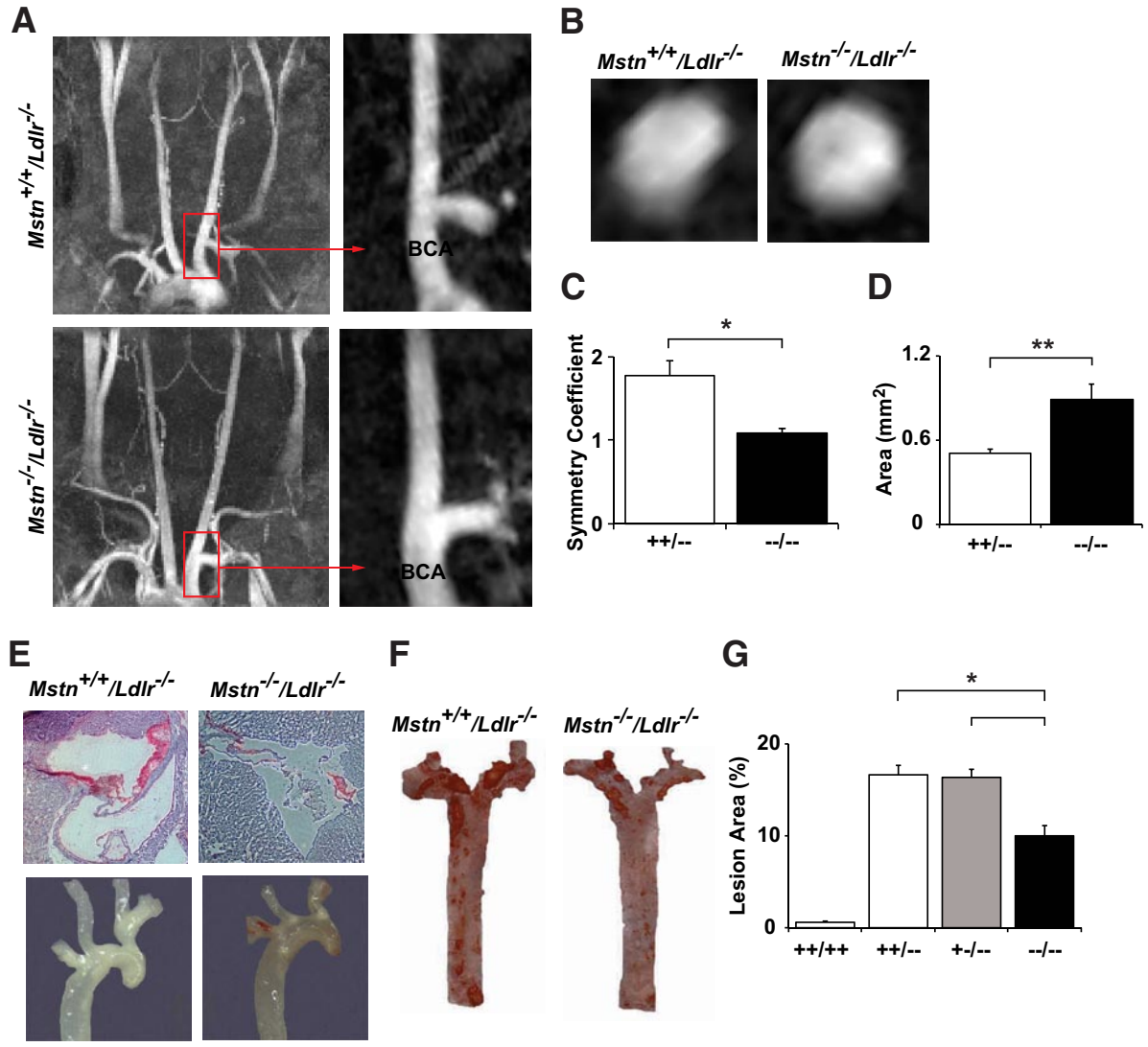

FIG. 2. Effects of *Mstn* disruption on atherogenesis progression in $Ldlr^{-/-}$ mice. *A*: Representative MRA of aortic arch and its major branches. BCA, brachiocephalic artery. *B*: Cross-sectional image of BCA. *C* and *D*: Symmetry coefficient (ratio of the largest to the smallest diameter) (*C*), and cross-sectional area (*D*) of BCA lumen (n = 4). *E*: Oil Red O staining of atherosclerotic lesions in aortic root at the level of the aortic valves (*top panel*). Magnification 40×. Gross aortic arch and branches (*bottom panel*) (n = 9–20). *F* and *G*: Sudan IV staining of *en face* aortas (*F*) and quantitative analyses of atherosclerotic lesion areas (percent of total aortic surface area) (*G*) (n = 9–20). $^{++/++}$, $Mstn^{+/+}/Ldlr^{+/+}$. $^{+-/--}$, $Mstn^{+/+}/Ldlr^{-/-}$. $^{+-/--}$, $Mstn^{+-}/Ldlr^{-/-}$. $^{--/--}$, $Mstn^{-/-}/Ldlr^{-/-}$. Data are expressed as means ± SE (n = 11–21). $^{**}P < 0.05$. $^{**}P < 0.01$. (A high-quality digital representation of this figure is available in the online issue.)

available in an online appendix). $Ldlr^{-/-}$ mice with heterozygous deletion of *Mstn* only displayed modest increase in muscle mass but have similar fat mass accumulation compared with $Mstn^{+/+}/Ldlr^{-/-}$ controls when fed HFD.

Despite the remarkable effects of *Mstn* deletion on body composition, neither the energy intake nor energy expenditure differed significantly among the various groups on normal rodent diet (data not shown) or on HFD (supplementary Fig. 2*A*, available in an online appendix). Ambulatory activity levels on HFD were assessed by infrared beam interruption, and notably, the horizontal ambulatory activity of $Mstn^{-/-}/Ldlr^{-/-}$ double-knockout group was 38% lower than that of controls (supplementary Fig. 2*B*, available in an online appendix). However, despite this reduction in activity, analysis of whole body O_2 consumption (Vo_2) showed that energy expenditure was similar between the two groups (supplementary Fig. 2*C*, available in an online appendix). If the data were expressed as a function of lean mass weight, $Mstn^{-/-}/Ldlr^{-/-}$ actually had lower Vo_2 rate (13%) compared with controls. Furthermore, the respiratory exchange ratios were ~0.85 in $Ldlr^{-/-}$ mice with or without *Mstn* disruption, reflecting mixed utilization of carbohydrate and fatty acid oxidation in both animal groups (supplementary Fig. 2*D*, available in an online appendix). Thus, the resistance to fat accumulation in $Mstn^{-/-}/Ldlr^{-/-}$ mice cannot be explained based on reduced food intake, increased whole-body O_2 consumption, or preference for fuel disposition.

***Mstn* deletion reduces diet-induced atherogenesis in $Ldlr^{-/-}$ mice.** To determine whether deletion of *Mstn* mitigates the development of vascular lesions, we first used in vivo MRA to evaluate lumen occlusion of the brachiocephalic artery, one of the most lesion-prone sites (Fig. 2*A*). After 8 weeks of HFD, $Mstn^{+/+}/Ldlr^{-/-}$ mice showed reduced lumen size and increased asymmetry (Fig. 2*B–D*); in contrast, brachiocephalic arterial lumen of $Mstn^{-/-}/Ldlr^{-/-}$ maintained patency without significant

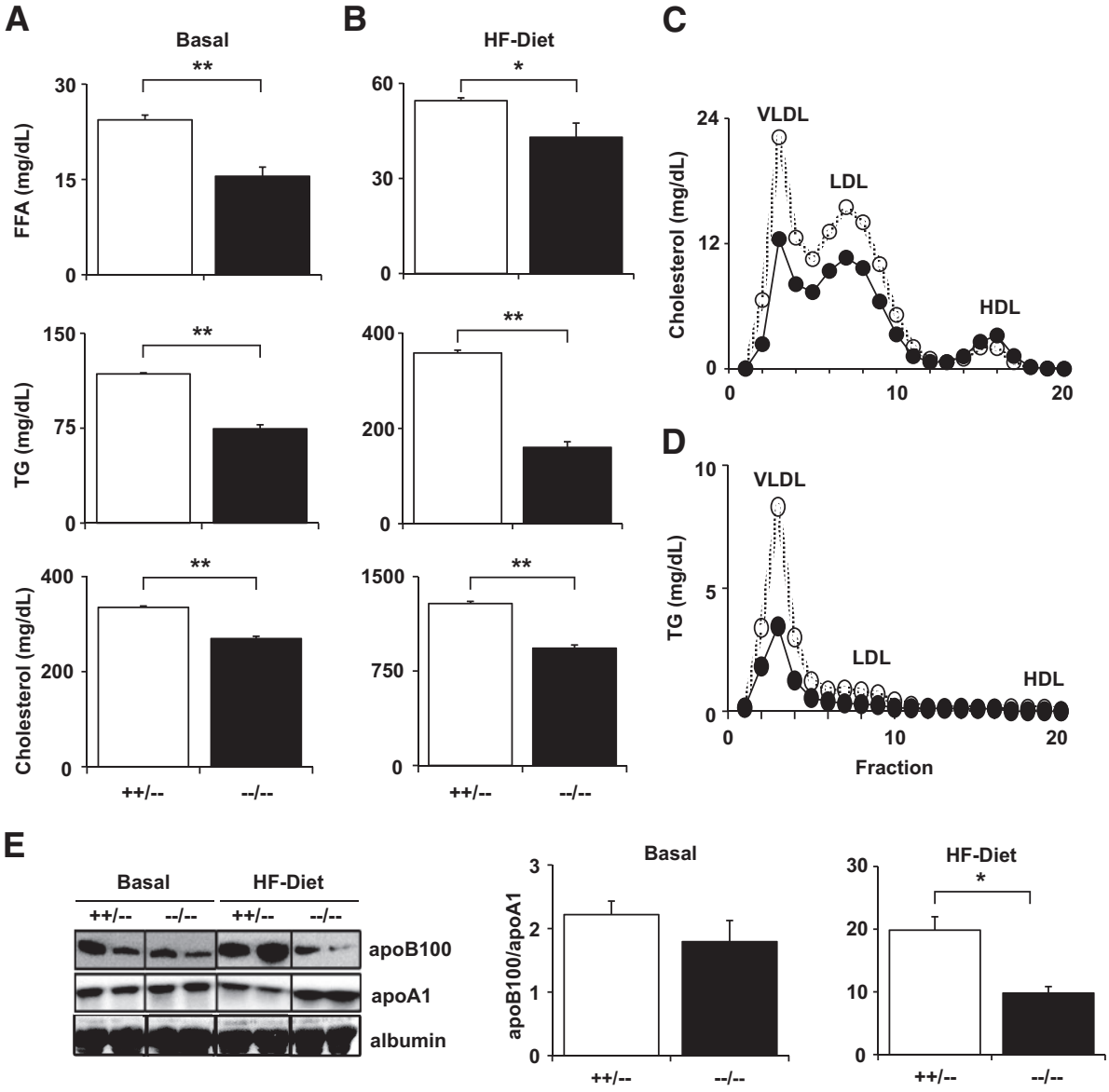

FIG. 3. Atherogenic lipid profile in $Ldlr^{-/-}$ mice with *Mstn* deletion. *A* and *B*: Fasting plasma FFA, triglycerides, and cholesterol levels of mice at baseline (*A*) and after 10 weeks of HFD (HF-diet) (*B*). *C* and *D*: Lipoprotein profile in $Mstn^{+/+}/Ldlr^{-/-}$ (○) and $Mstn^{-/-}/Ldlr^{-/-}$ (●) mice after 11 weeks of HFD. Data are presented as average cholesterol (*C*) and triglycerides (*D*) distribution for each group. *E*: Plasma apoA1- and apoB100-containing lipoprotein particles before and after induction of HFD. The graphs demonstrate the quantification of each molecule, displayed as apoB100/apoA1 ratio. Averages were taken from four different gels. Blood was drawn from mice after 10 weeks of HFD. $^{++/--}$, $Mstn^{+/+}/Ldlr^{-/-}$. $^{--/--}$, $Mstn^{-/-}/Ldlr^{-/-}$. Data are shown as the means ± SE (n = 7–10). *$P < 0.05$, **$P < 0.01$.

occlusion, as indicated by greater symmetry and significantly larger (1.7-fold) lumen area (Fig. 2*C* and *D*).

After 12 weeks of HFD, animals were killed and aortas were dissected. $Mstn^{+/+}/Ldlr^{-/-}$ mice developed large plaques that were eccentric (partial circumference of arterial wall) and dispersed along the arch and in the descending aorta (Fig. 2*E*). Staining with Oil Red O revealed that the lesions were lipid rich (Fig. 2*E*). Analysis of the *en face* aorta demonstrated that atheromatous lesion area in $Mstn^{-/-}/Ldlr^{-/-}$ mice was 41% lower than in $Mstn^{+/+}/Ldlr^{-/-}$ controls (Fig. 2*F* and *G*). In correlation with the similar fat mass accumulation (Fig. 1*B* and *C*), $Mstn^{+/-}/Ldlr^{-/-}$ mice had similar lesion area compared with $Mstn^{+/+}/Ldlr^{-/-}$ controls (Fig. 2*G*), suggesting that heterozygous deletion of *Mstn* is not sufficient in providing protection against either fat accumulation or atherogenesis. The negative control, $Mstn^{+/+}/Ldlr^{+/+}$ mice group, had no detectable lesions. Thus, $Ldlr^{-/-}$ mice with *Mstn* deletion were protected against the development/progression of atheromatous lesions.

We next investigated the mechanisms by which disruption of *Mstn* retards atherogenesis progression. As circulating lipids are important contributors to atherogenesis, we determined the changes in plasma lipids and lipoproteins.

***Mstn* deletion in $Ldlr^{-/-}$ mice attenuates proatherogenic dyslipidemia.** Even before HFD induction, $Mstn^{-/-}/Ldlr^{-/-}$ mice had significantly lower plasma triglycerides, free fatty acids (FFA), and total cholesterol levels compared with $Mstn^{+/+}/Ldlr^{-/-}$ mice (Fig. 3*A*). After 10 weeks of HFD, $Mstn^{+/+}/Ldlr^{-/-}$ controls displayed marked increase in plasma triglycerides (3.0-fold), FFA (2.3-fold), and cholesterol (3.8-fold) levels compared with baseline; the changes in plasma lipids were significantly greater

than those observed in *Mstn*$^{-/-}$/*Ldlr*$^{-/-}$ mice after HFD. Plasma triglycerides, FFA, and cholesterol levels after HFD were significantly lower in *Mstn*$^{-/-}$/*Ldlr*$^{-/-}$ than in *Mstn*$^{+/+}$/*Ldlr*$^{-/-}$ controls (Fig. 3*B*), suggesting that *Mstn* deletion protects against the development of proatherogenic dyslipidemia in *Ldlr*$^{-/-}$ mice fed HFD.

We fractionated plasma lipoproteins by using fast-phase liquid chromatography. Plasma total cholesterol, VLDL-cholesterol, and LDL cholesterol levels were lower in *Mstn*$^{-/-}$/*Ldlr*$^{-/-}$ mice than in *Mstn*$^{+/+}$/*Ldlr*$^{-/-}$ controls (Fig. 3*C*). Triglyceride contents of VLDL (VLDL-TG) and LDL fractions (LDL-TG) were also significantly lower in *Mstn*$^{-/-}$/*Ldlr*$^{-/-}$ mice than controls (Fig. 3*D*).

ApoB is an important predictor of cardiovascular risk; some patients with elevated apoB100 levels are at increased risk of cardiovascular disease despite having target cholesterol levels (18,19). We analyzed the plasma apoB100 contents in our mice. Western blot analysis of plasma samples of *Mstn*$^{+/+}$/*Ldlr*$^{-/-}$ mice showed a significant increase in apoB100 after 11 weeks of HFD, and this diet effect was markedly attenuated in *Mstn*$^{-/-}$/*Ldlr*$^{-/-}$ mice (Fig. 3*E*). We also measured apoA1, the scaffold protein for HDL. The ratio of apoB100 to apoA1, which is stoichiometrically related to the ratio of non-HDL to HDL particles, was lower in *Mstn*$^{-/-}$/*Ldlr*$^{-/-}$ mice compared with controls (Fig. 3*E*), suggesting a more favorable lipoprotein profile in *Mstn*$^{-/-}$/*Ldlr*$^{-/-}$ mice.

***Mstn*$^{-/-}$/*Ldlr*$^{-/-}$ mice have greater insulin-mediated glucose disposal.** Diet-induced obesity is strongly associated with deterioration of insulin sensitivity, clinically evidenced by increased circulating insulin, glucose, triglycerides, and FFA (20). Insulin also serves as an important regulator of adipose lipolysis and hepatic VLDL production. Dysregulation of these metabolic functions of insulin could contribute to hyperlipidemia and accelerate atherosclerosis in mice fed with HFD (21,22). Accordingly, we assessed the effect of *Mstn* deletion on insulin sensitivity in *Ldlr*$^{-/-}$ mice.

In addition to having lower plasma triglycerides, FFA, VLDL, and apoB concentrations, *Mstn*$^{-/-}$/*Ldlr*$^{-/-}$ mice also had significantly lower fasting blood glucose and insulin levels. These data suggested that *Mstn*$^{-/-}$/*Ldlr*$^{-/-}$ mice were more insulin sensitive than *Mstn*$^{+/+}$/*Ldlr*$^{-/-}$ controls even when fed HFD (Fig. 4*A*–*C*). Plasma insulin-to-glucagon ratio was also significantly lower (30% in *Mstn*$^{-/-}$/*Ldlr*$^{-/-}$ mice). Glucose tolerance test did not reveal significant differences between rate of glucose disposal (supplementary Fig. 3*A*, available in an online appendix), but this could be because of the compensatory increase in fasting insulin in *Mstn*$^{+/+}$/*Ldlr*$^{-/-}$ (Fig. 4*B*). When mice were injected with a fixed dose of insulin during insulin tolerance tests, *Mstn*$^{-/-}$/*Ldlr*$^{-/-}$ mice maintained significantly lower blood glucose than their *Mstn*$^{+/+}$/*Ldlr*$^{-/-}$ littermates (supplementary Fig. 3*B*, available in an online appendix). Furthermore, *Ldlr*$^{-/-}$ mice with *Mstn* deletion had significantly lower phosphoenolpyruvate carboxykinase one (*Pepck*) expression (supplementary Fig. 3*C*, available in an online appendix), the rate-limiting hepatic gluconeogenic enzyme (23), consistent with improved insulin sensitivity.

To confirm our findings of improved insulin sensitivity in *Mstn*$^{-/-}$/*Ldlr*$^{-/-}$ mice, we performed hyperinsulinemia-euglycemic clamp studies, the accepted gold standard for assessing insulin sensitivity (24). *Mstn*$^{-/-}$/*Ldlr*$^{-/-}$ required significantly higher GIR to maintain euglycemia (Fig. 4*D* and *E*) than in controls. These data demonstrate that *Mstn* deletion improves whole body insulin sensitivity through the enhancement of insulin-stimulated glucose disposal in peripheral tissues. It is possible that the increased GIR is simply because of greater muscle mass and the resulting increase in metabolic demand of the double-knockout mice. To explore this further, we measured the rates of [^{3}H]-2-deoxyglucose uptake in skeletal muscle during the clamp procedure. In the *Mstn*$^{-/-}$/*Ldlr*$^{-/-}$ mice, glucose uptake in *quadriceps* muscle was significantly higher compared with that of the *Mstn*$^{+/+}$/*Ldlr*$^{-/-}$ controls (Fig. 4*F*) in a similar hyperinsulinemic state (Fig. 4*G*). Furthermore, phosphorylation of serine-473 in Akt, the pleiotropic kinase essential for many metabolic actions of insulin, was significantly higher in muscle tissues of *Mstn*$^{-/-}$/*Ldlr*$^{-/-}$ mice compared with that of the controls. Phosphorylation of serine-21/9 in GSK3, one of Akt substrates, was also significantly higher, providing further evidence of improved insulin action in the skeletal muscle (Fig. 4*H*). Together, these data demonstrate that HFD induces an insulin-resistant state in *Mstn*$^{+/+}$/*Ldlr*$^{-/-}$ mice and that disruption of *Mstn* prevents the development of insulin resistance, as consistent with other reports (9,10).

***Mstn*$^{-/-}$/*Ldlr*$^{-/-}$ are protected against hepatic steatosis and have higher hepatic fatty acid β-oxidation and lower VLDL secretion rates.** The liver plays a leading role in systemic lipid homeostasis (25). In response to HFD feeding, the livers of *Mstn*$^{+/+}$/*Ldlr*$^{-/-}$ mice displayed substantial fat accumulation (Fig. 5*A*). In contrast, *Mstn*$^{-/-}$/*Ldlr*$^{-/-}$ mice had significantly lower hepatic triglyceride content, as well as total wet and dry liver weights (Fig. 5*A*; supplementary Fig. 4*A*, available in an online appendix). This protection against diet-induced hepatic fat infiltration in *Mstn*$^{-/-}$/*Ldlr*$^{-/-}$ mice was associated with significant reduction in plasma adipose-derived FFA (Fig. 3*A*), glucose, and insulin (Fig. 4*A* and *B*), as well as with diminished expression of lipogenic master gene, sterol regulatory element–binding transcription factor 1 (*Srebf1*), and its key downstream target, fatty acid synthase mRNA and protein (Fig. 5*B*–*D*).

Hepatic fatty acid β-oxidation has been shown to prevent diet-induced obesity, fatty liver, and hyperlipidemia (26). In our *Mstn*$^{-/-}$/*Ldlr*$^{-/-}$ mice model, hepatic fatty acid β-oxidation rates in isolated hepatic mitochondrion were significantly greater (1.7-fold; supplementary Fig. 4*B*, available in an online appendix) than those from controls. In addition, we have previously shown that *Mstn* deletion resulted in a 25% increase of liver mitochondrial DNA (unpublished data), implying that these mice have greater mitochondrial oxidation capacity. Plasma level of the ketone body β-hydroxybutyrate, an indirect marker of hepatic fatty acid β-oxidation, was also significantly higher in *Mstn*$^{-/-}$/*Ldlr*$^{-/-}$ (supplementary Fig. 4*C*, available in an online appendix) than in controls.

Decreased hepatic triglycerides in *Mstn*$^{-/-}$/*Ldlr*$^{-/-}$ mice was associated with reduced secretion of hepatic triglycerides (23%) and VLDL (Fig. 5*E*). Suppression of hepatic fat accumulation in *Mstn*$^{-/-}$/*Ldlr*$^{-/-}$ mice was associated with enhanced insulin action in the liver. The mRNA expression levels of insulin receptor substrate (Irs)1 and Irs2, two key players in the regulation of hepatic insulin signaling (27), were significantly higher in *Mstn*$^{-/-}$/*Ldlr*$^{-/-}$ mice compared with *Mstn*$^{+/+}$/*Ldlr*$^{-/-}$ controls (supplementary Fig. 4*D*, available in an

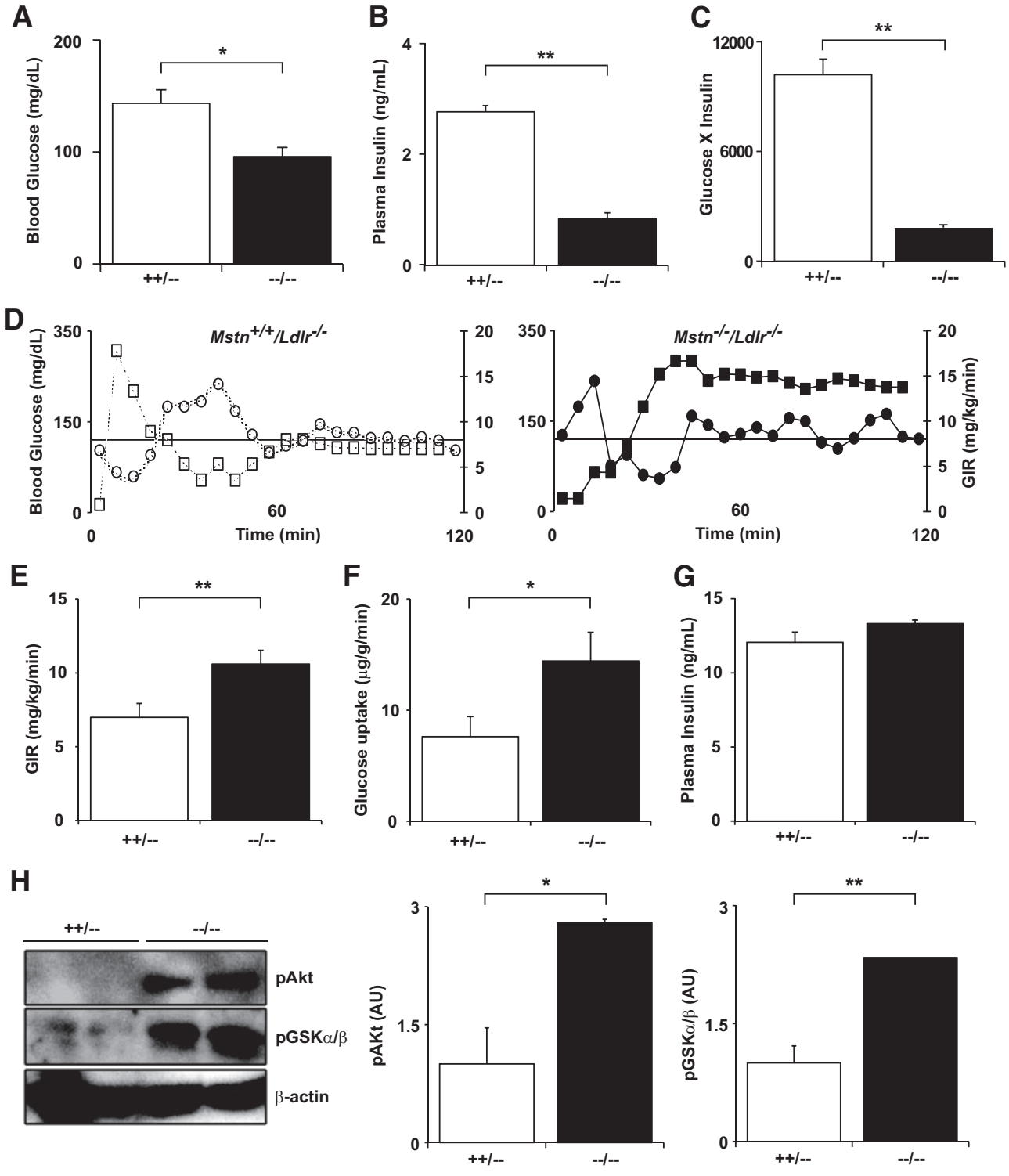

FIG. 4. Metabolic studies in $Ldlr^{-/-}$ mice with *Mstn* deletion. *A–C*: Fasting blood glucose (*A*), plasma insulin (*B*), and glucose (mg/dl) × insulin product (μIU/ml) ratio (*C*) of $Mstn^{+/+}/Ldlr^{-/-}$ and $Mstn^{-/-}/Ldlr^{-/-}$ mice after 8 weeks of HFD. *D–G*: Hyperinsulinemic-euglycemic clamp studies in mice after 12 weeks of HFD. Trace of blood glucose and GIR during the 2-h clamp (*D*) (○ and ●, blood glucose; □ and ■, GIR), average GIR (*E*), glucose uptake in quadriceps muscle (*F*), and average plasma insulin during clamp period (*G*). *H*: Akt serine-473 and GSKα/β serine-21/9 phosphorylation in the quadriceps muscle of mice. The graphs demonstrate the quantification of phosphorylated form of each molecule. Averages were taken from three different experiments. ++/−−, $Mstn^{+/+}/Ldlr^{-/-}$. −−/−−, $Mstn^{-/-}/Ldlr^{-/-}$. AU, arbitrary units. Data are shown as the means ± SE (n = 7–10). *$P < 0.05$, **$P < 0.01$.

online appendix). Western blot analyses also showed significantly higher Akt and GSK phosphoryation in isolated liver tissues of $Mstn^{-/-}/Ldlr^{-/-}$ mice (Fig. 5*F*). As emerging data suggest a causative role of intracellular hepatic triglyceride accumulation in the pathogenesis of hepatic insulin resistance and hypersecretion of VLDL (23,28–30), these findings provide a mechanistic link between the protective effects of *Mstn* deletion on obesity, insulin resistance, and atherosclerosis (supplementary Fig. 5, available in an online appendix).

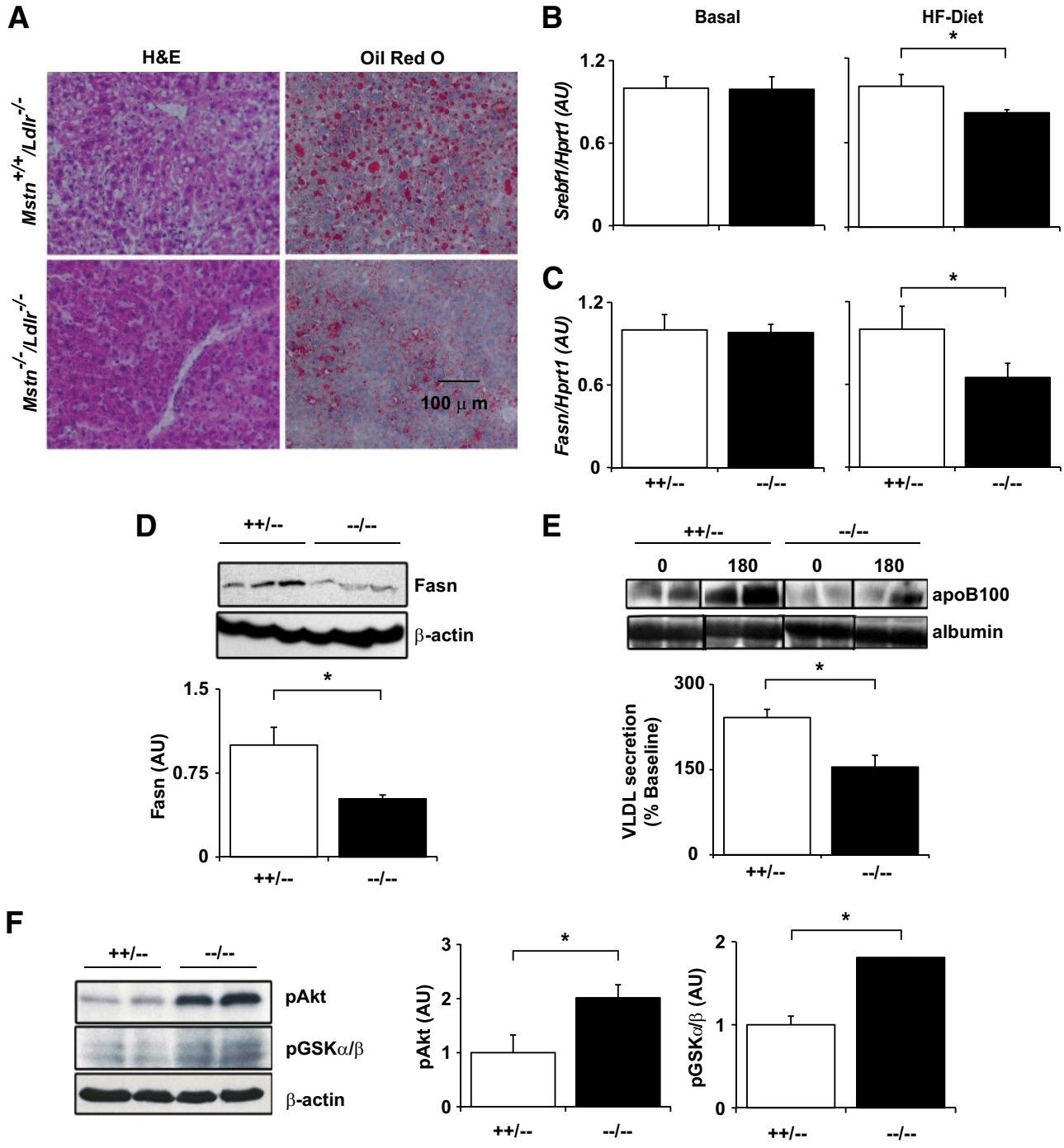

FIG. 5. Effects of *Mstn* deletion on liver of $Ldlr^{-/-}$ mice. *A*: Hematoxylin and eosin (H&E) and Oil Red O staining of the liver of $Mstn^{+/+}/Ldlr^{-/-}$ and $Mstn^{-/-}/Ldlr^{-/-}$ mice after 12 weeks of HFD (HF-diet). *B* and *C*: mRNA expression of *Srebf1* (*B*) and fatty acid synthase (*Fasn*) (*C*) in the liver of mice before and after 12 weeks of HFD. Values are expressed with respect to $Mstn^{+/+}/Ldlr^{-/-}$ controls. *D*: Protein expression of fatty acid synthase. Averages were taken from three different gels. *E*: Plasma apoB100 at 0 and 180 min after injection of Triton WR1339, a lipoprotein lipase inhibitor. VLDL secretion is determined as percent increase of apoB100 from baseline. Averages were taken from three different gels. *F*: Akt serine-473 and GSKα/β serine-21/9 phosphorylation in the liver of mice after 12 weeks of HFD. The graphs demonstrate the quantification of phosphorylation of each molecule. ++/−−, $Mstn^{+/+}/Ldlr^{-/-}$. −−/−−, $Mstn^{-/-}/Ldlr^{-/-}$. AU, arbitrary units. Data are shown as the means ± SE (n = 7–10). *$P < 0.05$, **$P < 0.01$. (A high-quality digital representation of this figure is available in the online issue.)

DISCUSSION

In this report, we provide the evidence that *Mstn* disruption in $Ldlr^{-/-}$ mice reduces the development of proatherogenic dysipidemia and atherogenesis progression. The $Mstn^{-/-}/Ldlr^{-/-}$ mice had lower plasma triglycerides, FFA, and non-HDL cholesterol than controls. $Mstn^{-/-}/Ldlr^{-/-}$ mice also had lower hepatic VLDL secretion rates. Although we cannot exclude direct actions of myostatin on the blood vessel wall, it is likely that the more favorable plasma lipid profile was the key contributor to reduced atherogenesis progression observed in $Mstn^{-/-}/Ldlr^{-/-}$ mice.

Mstn deletion prevented the development of diet-induced insulin resistance in $Ldlr^{-/-}$ mice. Hyperinsulinemic-euglycemic clamp studies revealed that $Mstn^{-/-}/Ldlr^{-/-}$ mice had significantly higher peripheral glucose

disposal rates. Furthermore, decreased circulating insulin as well as decreased glucose and adipose-derived FFA influx to the liver of the double-knockout mice may contribute to the protection against hepatic lipogenesis and hepatic insulin resistance (23,25,28).

The mechanisms by which *Mstn* deletion improves insulin sensitivity are not fully understood. *Mstn*$^{-/-}$/*Ldlr*$^{-/-}$ mice remained remarkably lean and resisted fat accumulation even when fed HFD for 12 weeks. Myostatin may exert complex effects on adipogenic differentiation (31,32). In addition, it is possible that acquisition of hypermuscularity by itself could lead to leanness (11). Indeed, mice with increased muscle oxidation, such as those overexpressing IGF-1 (33) or Akt-1 (11) in skeletal muscles, have little fat deposition. In our myostatin-deficient model, the marked hypertrophy of glycolytic skeletal muscle was associated with increased glucose uptake, lower blood glucose levels, and consequently lower circulating levels of insulin (11).

Increased hepatic fatty acid β-oxidation (FAO) and mitochondrial biogenesis with *Mstn* disruption may prevent the development of hepatic steatosis that was observed in *Mstn*$^{+/+}$/*Ldlr*$^{-/-}$ controls (25,26). Consistent with the higher FAO rates, *Mstn*$^{-/-}$/*Ldlr*$^{-/-}$ mice had higher ketone body production than controls. Improved insulin sensitivity might be expected to suppress FAO and lower ketone body production. However, insulin only effectively suppresses FAO in tissues, primarily muscle and fat, where glucose uptake is tightly regulated by insulin. Because hepatic glucose uptake is not regulated by insulin (34), improved insulin sensitivity in the *Mstn*$^{-/-}$/*Ldlr*$^{-/-}$ mice does not pose limitation on liver FAO as it does in the skeletal muscle. This phenomenon has also been observed by others (11,35). Our data suggest that the increased ketone body production in the double-knockout mice may be a result of physiological adaptation to limited adipose tissue storage for dietary fats from HFD.

Myostatin may also indirectly affect cardiometabolic risk by its effects on myokine secretion by the skeletal muscle. Similar to systemic loss of *Mstn*, inhibition of myostatin signaling exclusively in the skeletal muscle was sufficient to resist diet-induced obesity and insulin resistance (10). Myokines, such as interleukin-6, can alter metabolic states (36). Other myokines, such as fibroblast growth factor-21 (Fgf-21) and follistatin like-1 (Fstl-1), may also have salutary effects on fat accumulation and insulin sensitivity (37,38).

In summary, we have demonstrated here that *Mstn* deletion has beneficial cardiometabolic effects in an animal model of atherosclerosis. *Mstn*$^{-/-}$/*Ldlr*$^{-/-}$ mice are partially protected against not only fat accumulation and insulin resistance but also the development of proatherogenic dyslipidemia and atherosclerosis. These proof-of-concept studies raise the possibility that myostatin inhibitors may be useful agents for the prevention or treatment of atherosclerosis. Importantly, administration of myostatin inhibitors to humans have demonstrated specificity, safety, and effectiveness in increasing muscle mass and decreasing fat mass (39). To the extent that loss of skeletal muscle mass, adiposity, and atherogenesis occur contemporaneously during aging and in many chronic illnesses, new classes of promyogenic drugs, such as myostatin inhibitors, that increase skeletal muscle mass and retard fat accumulation are particularly attractive against these cardiometabolic disorders.

ACKNOWLEDGMENTS

We acknowledge the support of the U.S. National Institutes of Health grants RO1 DK49296, DK59261, DK64572, DK078512, DK72449, and T32 DK070201–31.

No potential conflicts of interest relevant to this article were reported.

We thank S.-J. Lee for the generous gift of *Mstn*$^{-/-}$ mice and Q. Yan for providing the training for the catheter placement surgery. We also thank L. Jiang, S. Wong, L. Kaoutzani, and E. Yang for valuable technical assistance.

REFERENCES

1. Sloan FA, Bethel MA, Ruiz DJ, Shea AM., MN F. The growing burden of diabetes mellitus in the US elderly population. Arch Intern Med 2008;168:192–199
2. Ding J, Kritchevsky SB, Newman AB, Taaffe DR, Nicklas BJ, Visser M, Lee JS, Nevitt M, Tylavsky FA, Rubin SM, Pahor M, Harris TB. Effects of birth cohort and age on body composition in a sample of community-based elderly. Am J Clin Nutr 2007;85:405–410
3. McPherron AC, Lawler AM, Lee SJ. Regulation of skeletal muscle mass in mice by a new TGF-beta superfamily member. Nature 1997;387:83–90
4. Amthor H, Huang R, McKinnell I, Christ B, Kambadur R, Sharma M, Patel K. The regulation and action of myostatin as a negative regulator of muscle development during avian embryogenesis. Dev Biol 2002;251:241–257
5. Artaza JN, Bhasin S, Magee TR, Reisz-Porszasz S, Shen R, Groome NP, Meerasahib MF, Gonzalez-Cadavid NF. Myostatin inhibits myogenesis and promotes adipogenesis in C3H 10T(1/2) mesenchymal multipotent cells. Endocrinology 2005;146:3547–3557
6. McPherron AC, Lee SJ. Suppression of body fat accumulation in myostatin-deficient mice. J Clin Invest 2002;109:595–601
7. Lee SJ. Regulation of muscle mass by myostatin. J Clin Invest 2004;20:61–86
8. Breslow JL. Mouse models of atherosclerosis. Science 1996;272:685–688
9. Wilkes JJ, Lloyd DJ, Gekakis N. A loss-of-function mutation in myostatin reduces TNF-α production and protects liver against obesity-induced insulin resistance. Diabetes 2009;58:1133–1143
10. Guo T, Jou W, Chanturiya T, Portas J, Gavrilova O, McPherron AC. Myostatin inhibition in muscle, but not adipose tissue, decreases fat mass and improves insulin sensitivity. PLoS ONE 2009;4:e4937
11. Izumiya Y, Hopkins T, Morris C, Sato K, Zeng L, Viereck J, Hamilton JA, Ouchi N, LeBrasseur NK, Walsh K. Fast/Glycolytic muscle fiber growth reduces fat mass and improves metabolic parameters in obese mice. Cell Metab 2008;7:159–172
12. Furuhashi M, Tuncman G, Gorgun CZ, Makowski L, Atsumi G, Vaillancourt E, Kono K, Babaev VR, Fazio S, Linton MF, Sulsky R, Robl JA, Parker RA, Hotamisligil GS. Treatment of diabetes and atherosclerosis by inhibiting fatty-acid-binding protein aP2. Nature 2007;447:959–965
13. Hedrick CC, Castellani LW, Warden CH, Puppione DL, Lusis AJ. Influence of mouse apolipoprotein A-II on plasma lipoproteins in transgenic mice. J Biol Chem 1993;268:20676–20682
14. Innis-Whitehouse W, Li X, Brown WV, Le NA. An efficient chromatographic system for lipoprotein fractionation using whole plasma. J Lipid Res 1998;39:679–690
15. Hruz PW, Murata H, Qiu H, Mueckler M. Indinavir induces acute and reversible peripheral insulin resistance in rats. Diabetes 2002;51:937–942
16. Folch J, Ascoli I, Lees M, Meath JA, Le BN. Preparation of lipide extracts from brain tissue. J Biol Chem 1951;191:833–841
17. Kuipers F, Jong MC, Lin Y, Eck M, Havinga R, Bloks V, Verkade HJ, Hofker MH, Moshage H, Berkel TJ, Vonk RJ, Havekes LM. Impaired secretion of very low density lipoprotein-triglycerides by apolipoprotein E-deficient mouse hepatocytes. J Clin Invest 1997;100:2915–2922
18. Lamarche B, Moorjani S, Lupien PJ, Cantin B, Bernard PM, Dagenais GR, Despres JP. Apolipoprotein A-I and B levels and the risk of ischemic heart disease during a five-year follow-up of men in the Quebec cardiovascular study. Circulation 1996;94:273–278
19. Walldius G, Jungner I, Holme I, Aastveit AH, Kolar W, Steiner E. High apolipoprotein B, low apolipoprotein A-I, and improvement in the prediction of fatal myocardial infarction (AMORIS study): a prospective study. Lancet 2001;358:2026–2033
20. Wellen KE, Hotamisligil GS. Inflammation, stress, and diabetes. J Clin Invest 2005;115:1111–1119
21. Ginsberg HN. Very low density lipoprotein metabolism in diabetes mellitus. Diabetes Metab Rev 1987;3:571–589
22. Malmstrom R, Packard CJ, Caslake M, Bedford D, Stewart P, Yki-Jarvinen

H, Shepherd J, Taskinen MR. Defective regulation of triglyceride metabolism by insulin in the liver in NIDDM. Diabetologia 1997;40:454–462
23. Shimomura I, Matsuda M, Hammer RE, Bashmakov Y, Brown MS, Goldstein JL. Decreased IRS-2 and increased SREBP-1c lead to mixed insulin resistance and sensitivity in livers of lipodystrophic and ob/ob mice. Mol Cell 2000;6:77–86
24. Leow MK, Addy CL, Mantzoros CS. Clinical review 159: Human immunodeficiency virus/highly active antiretroviral therapy-associated metabolic syndrome: clinical presentation, pathophysiology, and therapeutic strategies. J Clin Endocrinol Metab 2003;88:1961–1976
25. Lin J, Yang R, Tarr PT, Wu PH, Handschin C, Li S, Yang W, Pei L, Uldry M, Tontonoz P, Newgard CB, Spiegelman BM. Hyperlipidemic effects of dietary saturated fats mediated through PGC-1beta coactivation of SREBP. Cell 2005;120:261–273
26. Stefanovic-Racic M, Perdomo G, Mantell BS, Sipula IJ, Brown NF, RM OD. A moderate increase in carnitine palmitoyltransferase 1a activity is sufficient to substantially reduce hepatic triglyceride levels. Am J Physiol Endocrinol Metab 2008;294:E969–E977
27. Fritsche L, Weigert C, Haring HU, Lehmann R. How insulin receptor substrate proteins regulate the metabolic capacity of the liver–implications for health and disease. Curr Med Chem 2008;15:1316–1329
28. Kabir M, Catalano KJ, Ananthnarayan S, Kim SP, Van Citters GW, Dea MK, Bergman RN. Molecular evidence supporting the portal theory: a causative link between visceral adiposity and hepatic insulin resistance. Am J Physiol Endocrinol Metab 2005;288:E454–E461
29. Samuel VT, Liu ZX, Qu X, Elder BD, Bilz S, Befroy D, Romanelli AJ, Shulman GI. Mechanism of hepatic insulin resistance in non-alcoholic fatty liver disease. J Biol Chem 2004;279:32345–32353
30. den Boer M, Voshol PJ, Kuipers F, Havekes LM, Romijn JA. Hepatic steatosis: a mediator of the metabolic syndrome. Lessons from animal models. Arterioscler Thromb Vasc Biol 2004;24:644–649
31. Guo W, Flanagan J, Jasuja R, Kirkland J, Jiang L, Bhasin S. The effects of myostatin on adipogenic differentiation of human bone marrow-derived mesenchymal stem cells are mediated through cross-communication between Smad3 and Wnt/beta-catenin signaling pathways. J Biol Chem 2008;283:9136–9145
32. Feldman BJ, Streeper RS, Farese RV, Jr, Yamamoto KR. Myostatin modulates adipogenesis to generate adipocytes with favorable metabolic effects. Proc Natl Acad Sci U S A 2006;103:15675–15680
33. Musaro A, McCullagh K, Paul A, Houghton L, Dobrowolny G, Molinaro M, Barton ER, Sweeney HL, Rosenthal N. Localized Igf-1 transgene expression sustains hypertrophy and regeneration in senescent skeletal muscle. Nat Genet 2001;27:195–200
34. Thorens B, Charron MJ, HF L. Molecular physiology of glucose transporters Diabetes Care 1990;3:209–218
35. Abu-Elheiga L, Oh W, Kordari P, Wakil SJ. Acetyl-CoA carboxylase 2 mutant mice are protected against obesity and diabetes induced by high-fat/high-carbohydrate diets. Proc Natl Acad Sci U S A 2003;100:10207–10212
36. Pedersen BK, Akerstrom TC, Nielsen AR, Fischer CP. Role of myokines in exercise and metabolism. J Appl Physiol 2007;103:1093–1098
37. Izumiya Y, Bina HA, Ouchi N, Akasaki Y, Kharitonenkov A, Walsh K. FGF21 is an Akt-regulated myokine. FEBS Lett 2008;582:3805–3810
38. Ouchi N, Oshima Y, Ohashi K, Higuchi A, Ikegami C, Izumiya Y, Walsh K. Follistatin-like 1, a secreted muscle protein, promotes endothelial cell function and revascularization in ischemic tissue through a nitric-oxide synthase-dependent mechanism. J Biol Chem 2008;283:32802–32811
39. Wagner KR, Fleckenstein JL, Amato AA, Barohn RJ, Bushby K, Escolar DM, Flanigan KM, Pestronk A, Tawil R, Wolfe GI, Eagle M, Florence JM, King WM, Pandya S, Straub V, Juneau P, Meyers K, Csimma C, Araujo T, Allen R, Parsons SA, Wozney JM, Lavallie ER, JR. M. Phase I/IItrial of MYO-029 in adult subjects with muscular dystrophy. Ann Neurol 2008;65:543–545